Flexible-alkyl Tails Help Shape-matching and Close Packing in Self-assembly of

2	Supramolecular Structure
3	
4 5	Ping Liao ¹ , Steven P. Kelley ² , Kanishka Sikligar ² , Heng Deng ¹ , Gary A. Baker ² , Jerry L. Atwood ^{2*} , Jian Lin ^{1,3,4*}
6	¹ Department of Mechanical and Aerospace Engineering
7	² Department of Chemistry
8	³ Department of Electrical Engineering and Computer Science
9	⁴ Department of Physics and Astronomy
10	University of Missouri, Columbia, MO 65211, USA
11	*Email: <u>linjian@missouri.edu</u> and <u>atwoodj@missouri.edu</u>
12	Abstract
13	Due to the flexibility and bowl-shaped cavity, C-alkylpyrogallol[4]arenes (PgCn, where n represents the
14	length of alkyl chains) have garnered much attention over the past decade in supramolecular chemistry
15	Such cyclic polyphenolic compounds have been shown to be an excellent molecular building block
16	for self-assembly of a variety of crystalline materials and have been applied in many frontier
17	research areas ranging from ion transport, gas absorption/separation to biomedicine. In this work, we
18	demonstrate that the long flexible alkyl tails play a critical role in the self-assembly of PgCx. It is
19	found that they help the shape matching between the self-assembled building blocks and improve the
20	packing density, thus promoting formation of an unprecedented "tails-driven" supramolecular
21	structure. The successful demonstration of this work would pave a new route to self-assembly
22	materials by tuning the functional alkyl tails of the building blocks.
23	
24	
25	Inspired by the spontaneous and precise assembly of protein and DNA, rational design and synthesis
26	of functional materials via molecular self-assembly approach have attracted tremendous interest. ^{1, 2}

From small molecules to large particles, self-assembly shows its infinite potential in building ordered and well-controlled material structures.³⁻⁸ As one class of molecular building blocks, Pyrogallol[4]arene (PgC_x), a bowl-shaped macrocycle, is composed of 12 hydroxyl groups decorated on the upper-rim and 4 alkyl chain tails on the lower-rim. It can be developed into various self-assembled structures such as hydrogen-bonded nano-capsules, metal-organic nanocapsules (MONCs)¹⁰⁻¹² or nanotubes¹³ for potential applications in drug delivery¹⁴ and water purification.¹⁵ Typically, coordination-driven self-assembly of MONCs receives more attention due to the engagement of functional metal ions and versatile tunability through metal coordination. Recently, diverse dimeric and hexameric MONCs have been successfully discovered with various transition metal ions, such as Co²⁺, Fe²⁺, Ni²⁺. 10, 11, 16 However, in these studies, the most attention was paid on studying the roles of coordination chemistry of the metal ions with upper-rim hydroxyl groups in assembling structures with more complexity. Little work took the function of the lower-rim tails into consideration. 17, 18 In particular, the impact of the lower-rim tails on shape matching and packing density of the assembled PgC_x is To investigate this unanswered question, in this work we utilized still not clear. C-10-undecenal-pyrogallol[4] arenes (Pg C_{10} =, '=' denotes the carbon-carbon double bond at the terminal of the tails) to study the effects of long flexible alkyl tails on the shape matching and packing as well as disclosing the driving force that governs the self-assembly of PgC_x. Three main ways that contribute to this unique self-assembly manner are illustrated as follows. First, the 10-undecenal tails form a straight chain crystal analog layer, restricting the arrangement of the pyrogallol[4]arene. Second, in each PgC₁₀₌, one tail is filled into the formed pyrogallol[4]arenes crystal layer to compensate the shape mismatching, while the other three tails form the tails crystal,

1

2

3

4

5

6

7

8

9

10

11

12

13

14

15

16

17

18

19

20

21

which enriches the shapes selection for self-assembled building blocks. Third, the long undecanal tails help to lock the confirmation through dispersion interaction with the benzene rings on the pyrogallol[4] arenes so that the distribution of the PgC₁₀₌ is tightened. By these three ways, the self-assembled bilayer structure is more closely packed than the one that was previously reported.¹⁹ According to the NMR spectrum shown in Figure 1, the C-10-undecenal-pyrogallol[4]arene was successfully synthesized due to the high activation of aldehyde in the reaction with pyrogallol. All hydrogen atoms are well matched to the peaks. Carbon-carbon double bonds remained at the terminal of the tails. The sample was investigated by high-resolution mass spectrometry (HRMS). (Figure 2) The result showed the molecule weight of C-10-undecenal-pyrogallol[4] arene was 1104g/mol, which agreed to the assumed formula C₆₈H₉₆O₁₂. Energy dispersive X-ray spectroscopy (EDS) was used to test the mass and atom percentage of carbon and oxygen. (SI Figure 1 & SI **Table 1)** It showed the compound contained 73.7% carbon and 19.4% oxygen in mass, and 80.7% carbon and 15.9% oxygen in atoms, which matched to the formula C₆₈H₉₆O₁₂ within accepted error of EDS. By decoding SCXRD data, we can obtain details of the self-assembled structure (Figure 3&4). The crystal structure unit contains two C-10-undecenal-pyrogallol[4]arene molecules, five methanol molecules, and one water molecule. The crystal has surfactant-like packing where the 10-undecenal tails form an interdigitated bilayer. Each C-10-undecenal-pyrogallol[4] arene molecule has three tails that extend into the layer and one that is parallel to it. They can buffer the shape mismatch between the pyrogallol[4] arene. The polar –OH groups at the upper rim form a layer, which interacts with the methanol and water molecules through hydrogen bonding. One methanol molecule resides in the center of pyrogallol[4]arene. The aromatic pi circuit also appears to act as the hydrogen bond

1

2

3

4

5

6

7

8

9

10

11

12

13

14

15

16

17

18

19

20

21

1 acceptor for the –OH group.

2

3

4

5

6

7

8

9

10

11

12

13

14

15

16

17

18

19

20

21

22

In the previous work, ¹⁹ PgC₁ was self-assembled into a similar bilayer crystal structure. In that work, the distribution of PgC₁ strongly depended on 1-ethyl-3-methylimidazolium ethyl sulfate, the center guest, because the short one-carbon tails cannot limit the distribution of the pyrogallol[4]arenes. Interestingly, compared with PgC₁₀₌, PgC₁ has much shorter tails at the lower rim, which should reduce steric effects in the assembly. Thus, a smaller gap between the pyrogallol[4]arenes was expected. However, when the crystal unit was measured, it was found that the centroid-to-centroid distance between two PgC₁₀₌ is \sim 10.937 Å, but the one between two PgC₁ is \sim 12.328 Å. When investigated in detail, it is found that the PgC₁₀₌ macrocycles were distorted. In the direction of the tail that stretches into the pyrogallol[4]arene layer, the width of the macrocycles is ~8.4 Å, but in another direction, the width is ~11.2 Å (Figure 5a). Whereas, the widths of PgC₁ macrocycles are \sim 10 Å for both directions (**Figure 5b**). The carbon-carbon double bond at the terminus of the ligands plays the role of preventing the entertwining of the tails through distortion of the molecule chains to maintain the order of the tails. This work shows us that the long 10-undecenal tails play a critical role in assembling this closely packing self-assembled structure. As it is showed in the SCXRD result, in one crystal unit, one pyrogallol[4] arene forms hydrogen bonds with nearly all of the methanol and water molecules, whereas, another barely has interaction with these solvent molecules, which indicates that the locations of the pyrogallol[4]arenes do not depend on the distribution of the methanol or water molecules. Due to the short distance between two pyrogallol[4]arenes, one hydrogen bond is formed on the upper rim between the OH groups from different pyrogallol[4]arenes. Two water molecules combine two OH groups from two different pyrogallol[4] arenes, respectively. Compared with the result shown in the work done by Raston et. al., 20 these three hydrogen bonds are much weaker than the interaction between the heavy hydrophilic polar groups, which implies that the layer formed by the long tails makes the main contribution to the stability of this self-assembled system. The water and methanaol molecules are not aligned strictly as the metal ions in our previous research, 21, 22 because they do not need to control the conformation of the self-assembled system. One of the four long tails extends into the pyrogallol[4] arenes layer, buffering the shape mismatching and tightening the arrangement. Prismatic pyrogallol[4] arenes have gap between two lower rims, lowering the packing density, which is fulfilled by the long flexible alkyl tails in this work. Moreover, the alkyl tail and the nearby benzene ring keep a distance of 4-5Å, which is the dispersion interaction priority range. 23-26 In this way, the tail and pyrogallol[4] arene have a strong interaction, leading to the distortion of pyrogallol[4] arene. In the layer formed by the long undecanal tails, the tails have highly ordered distribution. Most of the angles of the carbon-carbon bond are in the 110-115° range, and all the tails are aligned in the same direction. This is a straight chain crystal analogs, ²⁷ which is one of the highest density distribution methods for the long alkyl chains. Due to the constrain of the tails, pyrogallol[4] arenes are packed more closely. There are various building block geometries in self-assembly, such as bars, 28 disks 29 as well as multipods,³⁰ but not all the geometries of the building blocks are suitable for the self-assembly. Thus, the attachment of soft ligands is used to adjust the distance and minimize the shape mismatch among the building blocks so that disordered assembly can be prevented.³¹ Whereas, there were still many limitations to increase the packing density because of the weak interlocking ability between the building blocks,³² and steric effect of the soft-ligands.²⁹ The tails in this assembled system are equal

1

2

3

4

5

6

7

8

9

10

11

12

13

14

15

16

17

18

19

20

21

- to the soft ligands in some published work. However, in this work, the location of the tails is well
- 2 designed, limiting the confirmation of the molecule chains, thus compensating the shape gap
- between the pyrogallol[4] arene. Therefore, in this structure, both the straight chain crystal and the
- 4 compensation of the shape gap designs are insightful ideas to increase the self-assembled structure
- 5 packing density.

Conclusion

6

- 7 The bilayer is strictly arranged by following the arrangement of the 10-undecenal tails crystal, which
- forms a "tails-driven" structure. In lots of published works, the arrangement of pyrogallol[4]arene
- 9 strongly relies on the covalent interactions between the guest center and the hydroxyls on the upper
- 10 rim. Whereas, in this work, the locations of the PgC_{10} do not rely on the covalent centers but are
- confined by their own tails so that they can assemble into free-standing nanocapsules or even more
- 12 complex structures. In addition, the tails that stretch into the PgC_{10} layer show that they can
- overcome the shape-mismatching between the assembled building blocks, which provides more
- options to build various types of self-assembled structures.³³ Also, the tails form a straight chain
- crystal analog to increase the packing density of the building blocks. From a molecule design
- perspective, this work paves a way to designing the self-assembly building blocks that can help to
- increase the packing density. It is also potentially insightful for the design of larger scale building
- blocks such as nanoparticles and macroparticles. In the future development, this design principle
- would help to assemble the guest free nanocapsules or drug delivery vehicles.

Acknowledgement

- 21 This work was finically supported by grants from National Science Foundation (Award number:
- 22 1825352 and 1933861).

Reference

- 3 (1) Aliprandi, A.; Mauro, M.; De Cola, L., Controlling and imaging biomimetic self-assembly. Nat. Chem.
- 4 **2016,** 8, (1), 10-15.
- 5 (2) Whitesides, G. M.; Grzybowski, B., Self-assembly at all scales. *Science* **2002**, 295, (5564), 2418-2421.
- 6 (3) Li, P. H.; Li, Y.; Zhou, Z. K.; Tang, S. Y.; Yu, X. F.; Xiao, S.; Wu, Z. Z.; Xiao, Q. L.; Zhao, Y. T.; Wang, H.
- 7 Y.; Chu, P. K., Evaporative Self-Assembly of Gold Nanorods into Macroscopic 3D Plasmonic Superlattice
- 8 Arrays. Adv. Mater. **2016**, 28, (13), 2511-2517.
- 9 (4) Black, C. T.; Murray, C. B.; Sandstrom, R. L.; Sun, S. H., Spin-dependent tunneling in self-assembled
- 10 cobalt-nanocrystal superlattices. *Science* **2000**, 290, (5494), 1131-1134.
- 11 (5) Talapin, D. V.; Shevchenko, E. V.; Bodnarchuk, M. I.; Ye, X. C.; Chen, J.; Murray, C. B., Quasicrystalline
- order in self-assembled binary nanoparticle superlattices. *Nature* **2009**, 461, (7266), 964-967.
- 13 (6) Shenton, W.; Pum, D.; Sleytr, U. B.; Mann, S., Synthesis of cadmium sulphide superlattices using
- self-assembled bacterial S-layers. *Nature* **1997**, 389, (6651), 585-587.
- 15 (7) Brunner, J.; Baburin, I. A.; Sturm, S.; Kvashnina, K.; Rossberg, A.; Pietsch, T.; Andreev, S.; Sturm, E.;
- 16 Colfen, H., Self-Assembled Magnetite Mesocrystalline Films: Toward Structural Evolution from 2D to 3D
- 17 Superlattices. *Adv. Mater. Interfaces* **2017**, 4, (1), 1600431.
- 18 (8) Paik, T.; Yun, H.; Fleury, B.; Hong, S. H.; Jo, P. S.; Wu, Y. T.; Oh, S. J.; Cargnello, M.; Yang, H.; Murray,
- 19 C. B.; Kagan, C. R., Hierarchical Materials Design by Pattern Transfer Printing of Self-Assembled Binary
- 20 Nanocrystal Superlattices. *Nano Lett.* **2017**, 17, (3), 1387-1394.
- 21 (9) Atwood, J. L.; Barbour, L. J.; Jerga, A., Organization of the interior of molecular capsules by hydrogen
- bonding. Proc. Natl. Acad. Sci. U.S.A. 2002, 99, (8), 4837-41.
- 23 (10) Hu, X.; Chai, J.; Zhang, C.; Lang, J.; Kelley, S. P.; Feng, S.; Liu, B.; Atwood, D. A.; Atwood, J. L.,
- 24 Biomimetic Self-Assembly of Co(II)-Seamed Hexameric Metal-Organic Nanocapsules. J. Am. Chem. Soc.
- 25 **2019,** 141, (23), 9151-9154.
- 26 (11) Rathnayake, A. S.; Fraser, H. W. L.; Brechin, E. K.; Dalgarno, S. J.; Baumeister, J. E.; White, J.;
- 27 Rungthanaphatsophon, P.; Walensky, J. R.; Kelley, S. P.; Barnes, C. L.; Atwood, J. L., Site-Specific Metal
- 28 Chelation Facilitates the Unveiling of Hidden Coordination Sites in an Fe(II)/Fe(III)-Seamed
- 29 Pyrogallol[4]arene Nanocapsule. J. Am. Chem. Soc. **2018**, 140, (46), 15611-15615.
- 30 (12) Rathnayake, A. S.; Fraser, H. W. L.; Brechin, E. K.; Dalgarno, S. J.; Baumeister, J. E.; White, J.;
- 31 Rungthanaphatsophon, P.; Walensky, J. R.; Barnes, C. L.; Teat, S. J.; Atwood, J. L., In situ redox reactions
- facilitate the assembly of a mixed-valence metal-organic nanocapsule. *Nat. Commun.* **2018**, 9, (1), 2119.
- 33 (13) Mossine, A. V.; Kumari, H.; Fowler, D. A.; Shih, A.; Kline, S. R.; Barnes, C. L.; Atwood, J. L., Ferrocene
- species included within a pyrogallol[4] arene tube. Chem. Eur. J. 2012, 18, (33), 10258-60.
- 35 (14) Fang, Y.; Lian, X.; Huang, Y.; Fu, G.; Xiao, Z.; Wang, Q.; Nan, B.; Pellois, J. P.; Zhou, H. C.,
- 36 Investigating Subcellular Compartment Targeting Effect of Porous Coordination Cages for Enhancing Cancer
- 37 Nanotherapy. Small **2018**, 14, (47), 1802709.
- 38 (15) Patil, R. S.; Zhang, C.; Sikligar, K.; Baker, G. A.; Atwood, J. L., Formation of Water Channels in the
- 39 Crystalline Hydrates of Macrocyclic Compounds. Chem. Eur. J. 2018, 24, (13), 3299-3304.
- 40 (16) Zhang, C.; Patil, R. S.; Liu, C.; Barnes, C. L.; Atwood, J. L., Controlled 2D Assembly of Nickel-Seamed
- 41 Hexameric Pyrogallol[4]arene Nanocapsules. J. Am. Chem. Soc. 2017, 139, (8), 2920-2923.
- 42 (17) Zhang, C.; Patil, R. S.; Li, T.; Barnes, C. L.; Teat, S. J.; Atwood, J. L., Preparation of Magnesium-Seamed

- 1 C-Alkylpyrogallol[4] arene Nanocapsules with Varying Chain Lengths. Chem. Eur. J. 2017, 23, (35),
- 2 8520-8524.
- 3 (18) Zhang, C.; Wang, F.; Patil, R. S.; Barnes, C. L.; Li, T.; Atwood, J. L., Hierarchical Self-Assembly of
- 4 Supramolecular Coordination Polymers Using Giant Metal-Organic Nanocapsules as Building Blocks. Chem.
- 5 *Eur. J.* **2018,** 24, (54), 14335-14340.
- 6 (19) Fowler, D. A.; Pfeiffer, C. R.; Teat, S. J.; Beavers, C. M.; Baker, G. A.; Atwood, J. L., Illuminating host-
- 7 guest cocrystallization between pyrogallol [4] arenes and the ionic liquid 1-ethyl-3-methylimidazolium
- 8 ethylsulfate. *CrystEngComm* **2014,** 16, (27), 6010-6022.
- 9 (20) Eggers, P. K.; Becker, T.; Melvin, M. K.; Boulos, R. A.; James, E.; Morellini, N.; Harvey, A. R.; Dunlop,
- 10 S. A.; Fitzgerald, M.; Stubbs, K. A., Composite fluorescent vesicles based on ionic and cationic amphiphilic
- 11 calix [4] arenes. RSC advances **2012**, 2, (15), 6250-6257.
- 12 (21) Wagle, D. V.; Kelley, S. P.; Baker, G. A.; Sikligar, K.; Atwood, J. L., An Indium-Seamed Hexameric
- 13 Metal-Organic Cage as an Example of a Hexameric Pyrogallol [4] arene Capsule Conjoined Exclusively by
- 14 Trivalent Metal Ions. *Angewandte Chemie* **2020**, 132, (21), 8139-8142.
- 15 (22) Shao, L.; Hua, B.; Hu, X.; Stalla, D.; Kelley, S. P.; Atwood, J. L., Construction of Polymeric Metal-
- Organic Nanocapsule Networks via Supramolecular Coordination-Driven Self-Assembly. Journal of the
- 17 American Chemical Society **2020**, 142, (16), 7270-7275.
- 18 (23) Strauss, M. A.; Wegner, H. A., Exploring London Dispersion and Solvent Interactions at Alkyl-Alkyl
- 19 Interfaces Using Azobenzene Switches. Angewandte Chemie International Edition 2019, 58, (51),
- 20 18552-18556.
- 21 (24) Pollice, R.; Chen, P., A Universal quantitative descriptor of the dispersion interaction potential.
- 22 Angewandte Chemie International Edition 2019, 58, (29), 9758-9769.
- 23 (25) Kruszynski, R.; Sierański, T., Can stacking interactions exist beyond the commonly accepted limits?
- 24 *Crystal Growth & Design* **2016,** 16, (2), 587-595.
- 25 (26) Grimme, S., Do special noncovalent π - π stacking interactions really exist? Angewandte Chemie
- 26 *International Edition* **2008,** 47, (18), 3430-3434.
- 27 (27) Franks, S.; Hartley, F. R., Preparation and properties of tertiary p-alkylarylphosphines containing
- straight-chain alkyl groups. Journal of the Chemical Society, Perkin Transactions 1 1980, 2233-2237.
- 29 (28) Wang, T.; Zhuang, J.; Lynch, J.; Chen, O.; Wang, Z.; Wang, X.; LaMontagne, D.; Wu, H.; Wang, Z.; Cao,
- 30 Y. C., Self-assembled colloidal superparticles from nanorods. *Science* **2012**, 338, (6105), 358-363.
- 31 (29) Ye, X.; Chen, J.; Engel, M.; Millan, J. A.; Li, W.; Qi, L.; Xing, G.; Collins, J. E.; Kagan, C. R.; Li, J.,
- 32 Competition of shape and interaction patchiness for self-assembling nanoplates. Nat. Chem. 2013, 5, (6),
- 33 466-473.
- 34 (30) Lin, H.; Lee, S.; Sun, L.; Spellings, M.; Engel, M.; Glotzer, S. C.; Mirkin, C. A., Clathrate colloidal
- 35 crystals. *Science* **2017**, 355, (6328), 931-935.
- 36 (31) Si, K. J.; Chen, Y.; Shi, Q. Q.; Cheng, W. L., Nanoparticle Superlattices: The Roles of Soft Ligands. Adv.
- 37 *Sci.* **2018,** 5, (1), 1700179.
- 38 (32) Wang, Q.; Wang, Z.; Li, Z.; Xiao, J.; Shan, H.; Fang, Z.; Qi, L., Controlled growth and shape-directed
- 39 self-assembly of gold nanoarrows. *Sci. Adv.* **2017,** 3, (10), 1701183.
- 40 (33) Gong, J. X.; Newman, R. S.; Engel, M.; Zhao, M.; Bian, F. G.; Glotzer, S. C.; Tang, Z. Y.,
- 41 Shape-dependent ordering of gold nanocrystals into large-scale superlattices. *Nat. Commun.* **2017**, 8, 14038.

42 Footnote

The crystal structure in this work can be found in CCDC: 2016347.

The published crystal data in reference 19 can be found in CCDC: 986741.

Figures and Caption

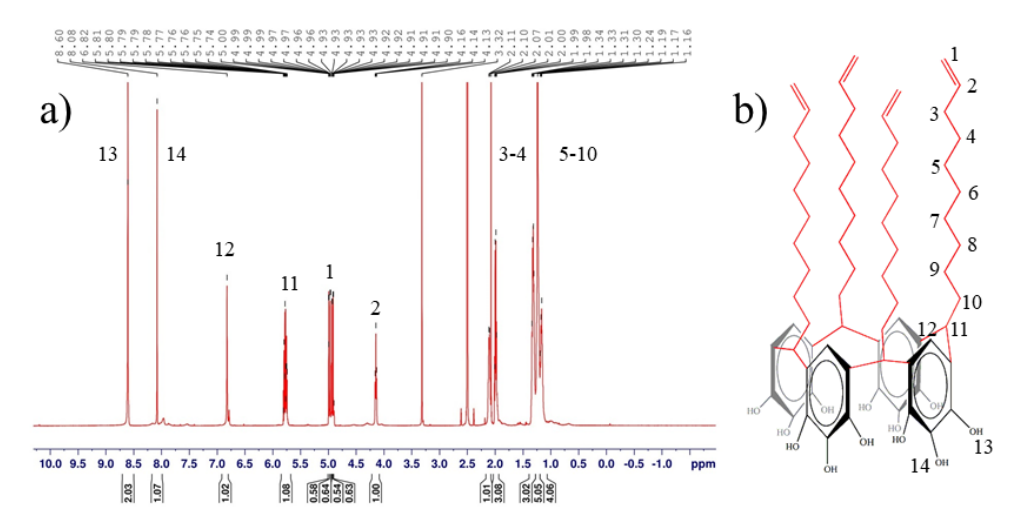


Figure 1. NMR result of synthesized C-10-undecenal-pyrogallol[4]arene (PgC₁₀₌). The signals at 2.5 ppm arise from DMSO. The one at 3.3 ppm is due to H_2O or HOD.

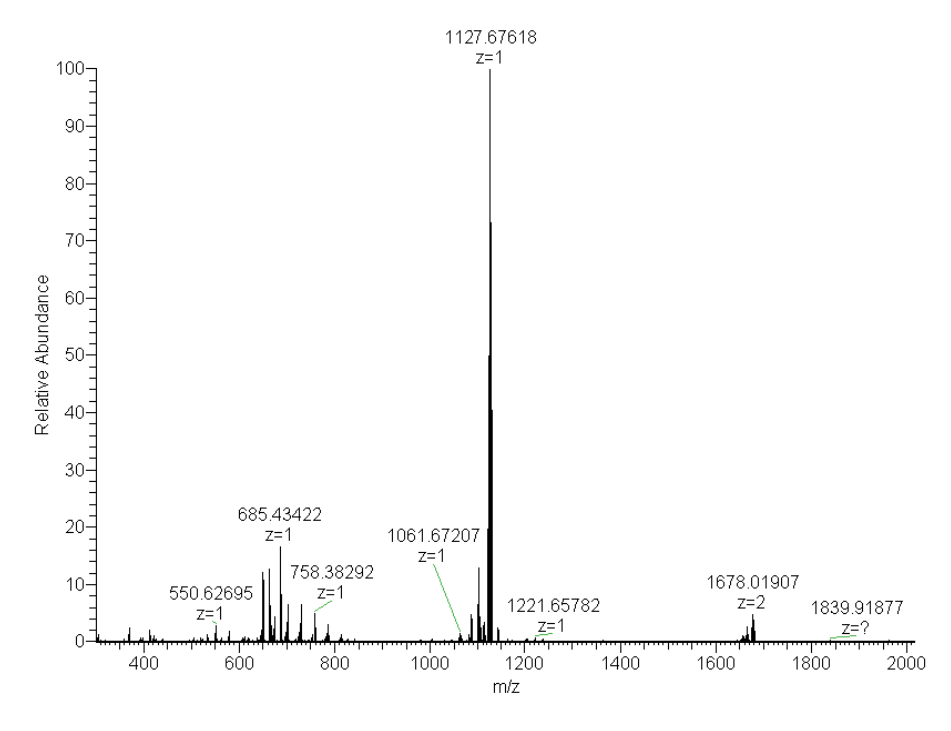


Figure 2. HRMS result. Summed and deconvoluted MS spectrum across 2 min acquisition. The highest abundance peak shows theoretical mass (+Na) is 1127 g/mol. When Na⁺ is removed, PGC₁₀₌ molecule weight is 1104 g/mol.

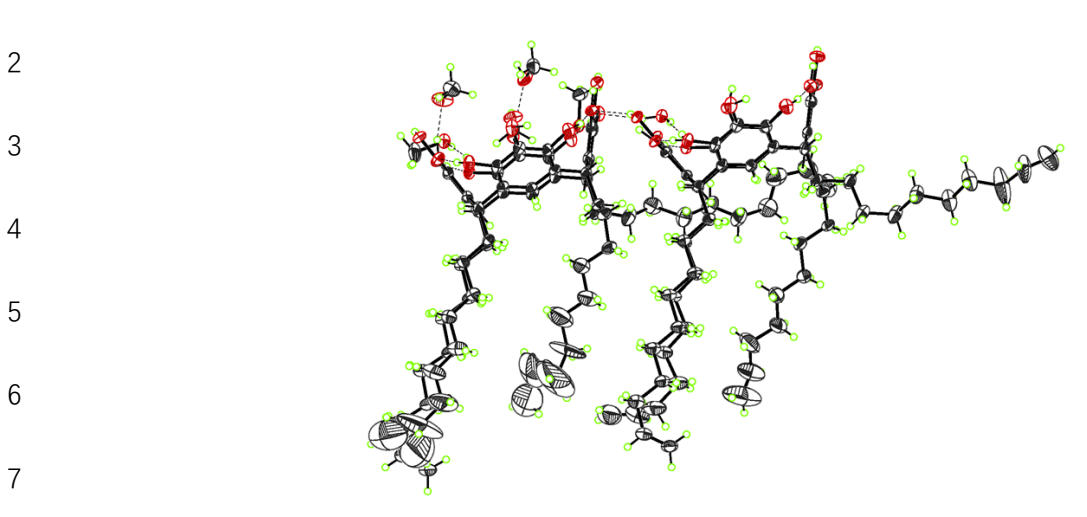


Figure 3. 50% probability ellipsoid plot of an asymmetric unit of PgC₁₀₌·2.5CH₃OH·H₂O. Color code: carbon: black, hydrogen: green, oxygen: red.

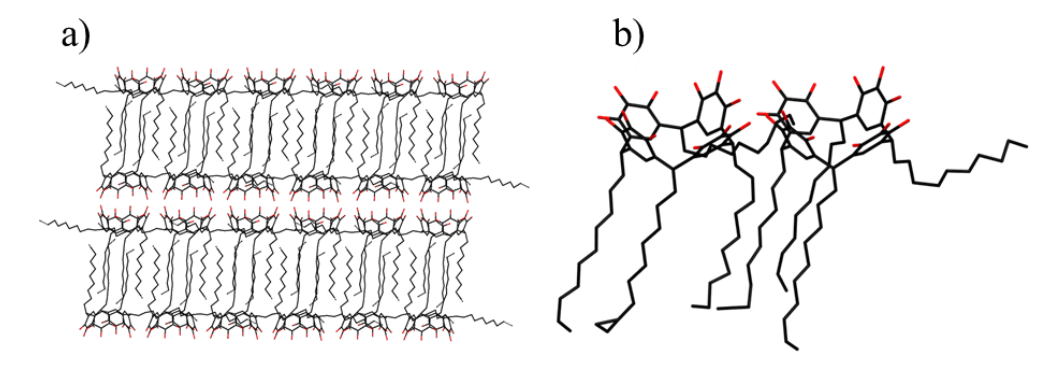
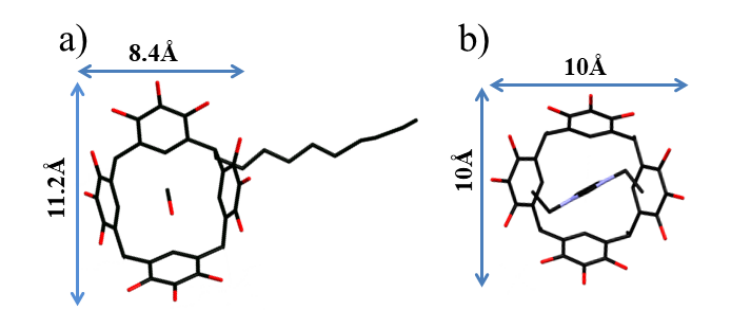


Figure 4. a) Schematic of a self-assembled bilayer structure from C-10-undecenal-pyrogallol[4] arene (PgC₁₀₌). Water, methanol molecules are removed from the schematic for better illustration. **b)** A unit cell of the self-assembled crystal. Color code: C: black; O: red; hydrogen atoms are removed.



- Figure 5. Crystal dimensions of a) PgC₁₀₌ and b) PgC₁ in their self-assembled structures. Color code: C: black,
- 2 O: red, N: purple. Irrelative ligand tails are removed.

1 Materials and Methods

- 2 All chemicals were purchased for use without subsequent purification.
- 3 Synthesis of C-10-undecenal-pyrogallol[4]arene: 33.6 g (0.2 mol) 10-undecenal and 25.22 g (0.2
- 4 mol) pyrogallol were dissolved into 200 mL ethanol. 12 mL saturated hydrochloric acid was added as
- 5 catalyst. The solution was heated with stirring for 24 h at 60 °C. After reaction, a red oily mixture
- 6 was obtained and then poured into 1 L acetonitrile and stirred thoroughly at 40 °C before cooling
- 7 down at 0 °C for half an hour. The C-10-undecenal-pyrogallol[4] arene was precipitated out of the
- 8 solvent. After filtration and drying the C-10-undecenal-pyrogallol[4] arene powder was obtained. The
- 9 yield was calculated with the formula below:

$$yield = \frac{mass \ of \ PGC_{10}}{mass \ of \ pyrogallol + mass \ of \ 10_undecenal} * 100\%$$

- 11 Where:
- 12 mass of $PGC_{10} = 25.2g (0.032mol)$,
- mass of pyrogallol = 25.22g (0.2mol),
- mass of 10-undecenal = 33.6g (0.2mol).
- 15 Therefore, the yield was 42.8% in mass.
- Assembly of bilayer structures: 300 mg C-10-undecenal-pyrogallol[4]arene powder was dissolved
- into 3 mL methanol under stirring and short time sonication. The solution was then evaporated
- slowly at room temperature for ~ 1 day. During the evaporation, C-10-undecenal-pyrogallol[4] arene
- 19 molecules were assembled into crystals. The crystals were collected for single-crystal X-ray
- 20 diffraction investigation directly.

Material characterization:

21

Nuclear magnetic resonance (NMR) testing was performed using a Bruker Avance III 600 MHz

spectrometer. ~10 mg C-10-undecenal-pyrogallol[4]arene powder was dissolved in deuterated 1 DMSO, and then tested by NMR. 2 3 Single crystal X-ray diffraction (XRD) data of PgC₁₀₌ crystals were collected on a Bruker Apex II diffractometer equipped with a CCD area detector (Bruker Nano, Inc., Madison, WI, USA) using 4 Mo-Ka radiation ($\lambda = 0.71073$ Å). The crystal was cooled to 100 K under a cold stream of N₂ gas 5 using a Cryostream 700 cryostat (Oxford Cryosystems, Oxford, UK). A hemisphere of unique data 6 7 was collected using a strategy of scans about the omega and phi axes. Unit cell determination, data collection, data reduction, absorption correction, and scaling were all performed with the Bruker 8 9 Apex3 software suite (Apex3, AXScale, and SAINT, version 2017.3-0, Bruker AXS, Inc., Madison, WI, 2017). 10 The structure of PgC₁₀₌ as shown in Figure 1 was solved by direct methods as implemented in 11 12 SHELXS (Sheldrick, G. M. SHELXS, v.2013-1, 2013) and refined by full-matrix least squares refinement using SHELXL-2017. Olex2 was used for structure visualization and model building.² 13 All non-hydrogen atoms were located from the difference map. Full occupancy atoms were refined 14 15 anisotropically. Hydrogen atoms bonded to carbon were placed in calculated positions, and their coordinates and thermal parameters were constrained to ride on the carrier atoms. Hydrogen atoms 16 on O-H groups were located from the difference map, and their coordinates were refined with the 17 O-H distances constrained to 0.92Å while the thermal parameters were constrained to ride on the 18 19 carrier atoms. Several of the 10-dodecenyl chains were disordered; in some cases this disorder appears to be too 20 severe to model atomically. Disordered chains were refined with distance restraints on the C-C and 21

C=C bonds (1.54 and 1.33 angstroms, respectively), and the anisotropic displacement parameters for

all atoms were restrained to be equal in magnitude along the covalent bonds. For chains that refined to extremely non-ideal geometries, the connectivity table was modified to remove unrealistic bonds so that hydrogen atom positions could be calculated. The major parts of all disordered chains could be refined anisotropically, and for chains with extremely distorted geometries, the large thermal ellipsoids likely indicate the region over which several highly overlapping disordered conformers occur. Hydrogen atoms could be located from the difference map for all O-H groups except for two of the methanol molecules and two of the pyrogallol oxygen groups. These were refined with the O-H distances restrained to 0.92 angstroms and the H atom thermal coordinates constrained to ride on the oxygen atoms. All O-H groups for which H atoms could not be found are associated with a portion of the hydrogen bonding network involving a methanol molecule with disordered oxygen atom positions; this should result in a corresponding disorder of the H atom positions for all the hydrogen bond donors. Since these H atoms could not be resolved from the difference map or inferred from the molecular geometry, they were left out of the model entirely and are assumed in the formula. High-resolution mass spectrometry (HRMS): Samples were dissolved in methanol (10ug/ml). Static nanospray was conducted on an LTQ Orbitrap. Data were acquired by HRMS (30,000 resolutions, FTMS, 2min acquisition). Data were examined with Qual Browser (V2.1). The sample was loaded into a static nanospray ECONO 12 tip (Proxeon) and analyzed by nano-electrospray ionization in positive-ion mode on a ThermoScientific LTQ Orbitrap XL mass spectrometer. Typical flow rates from these tips are estimated to be 50nL/min. FTMS data were collected in the Orbitrap (30,000 resolving power, 300-2000 m/z, 1 microscan, maximum inject time of 100ms) over 2min of infusion.

1

2

3

4

5

6

7

8

9

10

11

12

13

14

15

16

17

18

19

20

21

- 1 Energy dispersive X-ray spectroscopy (EDS): The crystallized sample was dried in vacuum
- 2 overnight under 60°C, and tested by FEI Quanta 600 FEG Environmental Scanning Electron
- 3 Microscope (ESEM) with Bruker Quantax 200 Silicon Drift Detector with Xflash6. The data was
- 4 processed in Bruker Esprit system. The sample was sitting on an Al stub during the test. We used 5
- and 20 kV voltage to obtain the spectrum. The data from 7 spectrum points were used to calculate the
- 6 average of the mass and atom percentage of carbon and oxygen. (SI Table 1)

9

10

11

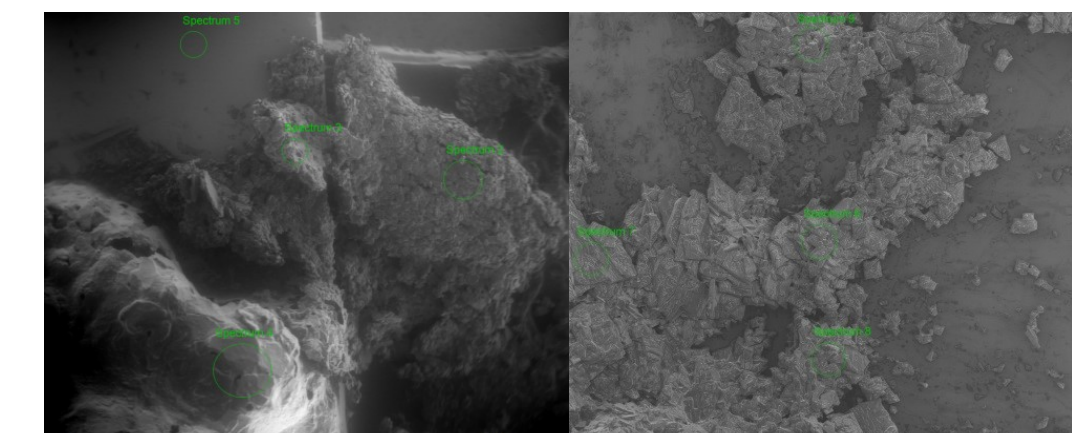
- 1. G. M. Sheldrick, Acta Crystallogr. C, 2015, 71, 3-8.
- 2. O. V. Dolomanov, L. J. Bourhis, R. J. Gildea, J. A. Howard and H. Puschmann, *J. Appl. Crystallogr.*, 2009, 42, 339-341.

121314

1617

15

18



19 20

SI Figure 1. Calculated points in EDS analysis (spectrum 2, 3, 4, 6, 7, 8, 9 were counted).

21

mass%										
element	speactrum-2	speactrum-3	speactrum-4	speactrum-6	speactrum-7	speactrum-8	speactrum-9	average		
carbon	70.54	71.91	73.73	74.15	75.66	73.88	76.08	73.7071		
oxygen	22.36	22.16	20.05	17.04	17.48	16.98	19.68	19.3929		
atom%										
element	speactrum-2	speactrum-3	speactrum-4	speactrum-6	speactrum-7	speactrum-8	speactrum-9	average		
carbon	77.59	78.52	80.21	81.6	82.48	81.64	82.66	80.6714		
oxygen	18.46	18.16	16.74	14.08	14.31	14.08	15.5	15.9043		

1 SI Table 1. Mass and atom percentage of carbon and oxygen for each spectrum.